Wave-packet analysis of interference patterns in output coupled atoms

Kari Härkönen,* Otto Vainio, and Kalle-Antti Suominen

Turku Centre for Quantum Physics, Department of Physics and Astronomy, University of Turku, FI-20014 Turku, Finland

(Received 22 February 2010; published 29 April 2010)

We study the output coupling of atoms from a magnetic trap into a linear potential slope of gravity using a weak radio-frequency field. We present a one-dimensional wave-packet model based on a continuous loading of a continuous spectrum of generalized eigenstates to describe the scenario. Analyzing the model, we show how the interference of the classical coupling fields maps to the interference of the resulting atomic streams.

DOI: 10.1103/PhysRevA.81.043638 PACS number(s): 03.75.Pp, 03.65.Sq

I. INTRODUCTION

Ever since the first realization of an atomic Bose-Einstein condensate [1–5], there have been applications where the coherent cloud of trapped atoms has been used as a source for output coupling [6]. The coherence properties of the source can be mapped to a coherent output [7,8] and, moreover, by applying continuous coupling a coherent stream of spatially widespread atoms can be created [9,10]. In a close analogy with the optical laser, an atom laser is thus formed.

A method used often to realize such a system is to induce spin flips to the trapped cloud of atoms by introducing a weak magnetic field perturbation (i.e., an oscillating rf field) perpendicular to the static trapping field [6,11,12]. The rf field creates a coupling between the Zeeman sublevels M_F, and the internal spin state can thus be flipped to an untrapped state or even, with strong rf-field intensities, to antitrapped states [13,14]. Especially in the linear Zeeman shift regime, the sublevel $M_F = 0$ does not couple to the static trapping magnetic field at all; it is only affected by the linear potential slope of the gravity. Consequently, such atoms fall freely and exit the trapping area. Other implementations of the output coupling include, for example, applying a Raman transition [15], which could also provide the free-falling atomic flux with an initial momentum kick, or constructing a tunneling connection [16]. Interestingly, the output coupling situation is reminiscent of the molecular dissociation triggered by ultrashort pulses [17–19].

Over the years, there have been theoretical papers that considered atomic lasers with one-dimensional [20–22] and three-dimensional models [12,23,24], using weak [11,25,26] and strong [11,22,27,28] coupling strengths, applying multiple simultaneous couplings [21,23], having the source at finite temperature [25,26], and from the point of view of stability [27–29] and pulse shape [30]. In this paper we analyze a simple one-dimensional model in order to clarify one specific problem concerning interference patterns due to multiple simultaneous couplings.

The phase coherence of the spatially elongated atomic beams is most strikingly demonstrated by strong interference patterns while superimposing two beams with different energies [31–33]. Again in a close analogy with the optical lasers, the interference pattern depends on three quantities: (i) the relative amplitudes, (ii) the relative phase difference, and (iii) the energy separation.

The spatially widespread wave-function interpretation of the interfering atomic beams is a strongly nonclassical result. However, an alternative explanation in terms of interfering (classical) magnetic rf fields, which drive the coupling, has been proposed [33]. In this line of reasoning, the coupling magnetic field is understood in terms of a carrier frequency and a beating envelope, and the correspondence between the pulsing rf amplitude and the resulting output stream was demonstrated. There seems to be a discrepancy between the two ways of looking at the problem. On the one hand, the system is described by a pulsing flux generated by a pulsing semiclassical coupling; on the other hand, the system is described by interference of superimposed spatially elongated asymptotic atomic wave functions [21,31]. The purpose of this paper is to demonstrate the connection between these two extreme interpretations.

In Sec. II we derive a wave-packet solution to a simplified one-dimensional problem in terms of a continuous loading of a continuous spectrum of generalized energy eigenstates. In Sec. III we show how the visibility of the atomic interference pattern maps from the interference of the magnetic fields. We then apply the model in Sec. IV using realistic experimental parameters and compare the results with numerical simulations, including the complete Zeeman-sublevel structure as well as the atomic contact interactions. Finally, we finish with conclusions and discussion in Sec. V.

II. WAVE-PACKET MODEL

A. Physical system

An atom couples to the magnetic field via its magnetic moment, resulting in an interaction energy defined as

$$U(\mathbf{B}) = -\boldsymbol{\mu} \cdot \mathbf{B}, \qquad (1)$$

where the magnetic moment operator is $\boldsymbol{\mu} = -\mu_0(g_S\mathbf{S} + g_L\mathbf{L} + g_I\mathbf{I})/\hbar$, and where $\mu_0 = |e|\hbar/2m_e$ is the Bohr magneton and g_i are the Landé g factors for electronic spin (S), orbital (L), and nuclear spin (I) angular momentum. When the energy splitting corresponding to this term is small compared to fine and hyperfine splittings, the total angular momentum $\mathbf{F} = \mathbf{I} + \mathbf{J}$, with $\mathbf{J} = \mathbf{L} + \mathbf{S}$, is a good quantum number and $\boldsymbol{\mu} \simeq -\mu_0 g_F \mathbf{F}/\hbar$, where the Landé factor is $g_F \simeq g_J[F(F+1) + J(J+1) - I(I+1)]/2F(F+1)$, with $g_J \simeq 1 + [J(J+1) + S(S+1) - L(L+1)]/2J(J+1)$. In the

*Present address: Department of Physics and Astronomy, University of Sussex, Brighton BN1 9QH, United Kingdom; Kari.Harkonen@utu.fi

limit of a weak magnetic field, which is the case in the present work, the Zeeman splitting between the sublevels M_F is linear [34].

1. Trapping potential and gravity

A magnetic trap for the atoms in the low-field-seeking states is formed by simply creating a magnetic field intensity minimum. The local direction of the field describes the quantization axis $\hat{\mathbf{e}}_z$, and, close to the minimum, the magnetic field is assumed to be approximately harmonic, such that $\mathbf{B}_{\text{trap}} = B_{\text{trap}}(\mathbf{r})\hat{\mathbf{e}}_z = B^0_{\text{trap}}(\lambda_x^2 x^2 + \lambda_y^2 y^2 + \lambda_z^2 z^2)\hat{\mathbf{e}}_z$. In the same direction, a strong static bias field $\mathbf{B}_{\text{bias}} = B_{\text{bias}}\hat{\mathbf{e}}_z$ is applied in order to remove the degeneracy at origin and, hence, to suppress the Majorana spin flips and the resulting atom losses [5].

The trapping potential operator is $U_{\text{trap}}(\mathbf{r}) = \text{sgn}(g_F)[\frac{1}{2}m(\omega_x^2 x^2 + \omega_y^2 y^2 + \omega_z^2 z^2) + \hbar\omega_{\text{bias}}]F_z/\hbar$, where $\omega_i^2 = 2\mu_0|g_F|B^0_{\text{trap}}\lambda_i^2/m$ and $\omega_{\text{bias}} = \mu_0|g_F|B_{\text{bias}}$. The atoms are also affected, irrespective of their internal state, by the linear potential of the gravity, $U_{\text{gravity}}(\mathbf{r}) = -mgx$; the harmonic trapping potentials are relocated accordingly in position and energy. The static Hamiltonian reads

$$H_0 = T + U_{\text{trap}}(\mathbf{r}) + U_{\text{gravity}}(\mathbf{r}), \tag{2}$$

where $T = -\hbar^2\nabla^2/2m$ is the kinetic energy term. As is now obvious, an integer-valued hyperfine state F supports a special sublevel $M_F = 0$, which is affected by only the linear gravitational potential.

2. Coupling rf field

The coupling between the Zeeman sublevels is induced by applying a weak rf field

$$\mathbf{B}_{\text{rf}}(t) = \tfrac{1}{2}B_0(t)\hat{\mathbf{e}}_{\text{rf}}e^{-i(\omega_{\text{rf}}t+\theta)} + \text{c.c.} \tag{3}$$

with a finite component in the direction perpendicular to the trapping field. The pulse envelope $B_0(t)$ has an arbitrary shape and the pulse is turned on after the initial time $t = 0$. As will be clear from the following, the model can be generalized directly to any linear combination of such single-mode rf fields. Consequently, it is sufficient now to consider a single rf field.

The rf field results in an interaction Hamiltonian

$$H_I(t) = -\boldsymbol{\mu}\cdot\mathbf{B}_{\text{rf}}(t). \tag{4}$$

We write the polarization vector as $\hat{\mathbf{e}}_{\text{rf}} = \sum_{i=+,-,z}(\hat{\mathbf{e}}_i\cdot\hat{\mathbf{e}}_{\text{rf}})\hat{\mathbf{e}}_i$, where $\hat{\mathbf{e}}_\pm = (\hat{\mathbf{e}}_x \pm i\hat{\mathbf{e}}_y)/\sqrt{2}$. The z component causes only a small perturbation in the trapping potential and is assumed to be zero hereafter. The circular components, corresponding to the raising and lowering angular momentum operators $F_\pm = F_x \pm iF_y$, induce transitions between the sublevels, as $F_\pm|F,M_F\rangle = \hbar\sqrt{F(F+1) - M_F(M_F \pm 1)}|F,M_F \pm 1\rangle$. Finally, we remark that the total angular momentum operator F^2 commutes with the total Hamiltonian $H(t) = H_0 + H_I(t)$ as well as its components H_0 and $H_I(t)$, so the dynamics is confined to a single hyperfine state F.

B. Representation of the state

The coupling is assumed to be weak, so only transitions to sublevels $M_{F,\text{final}} = M_{F,\text{initial}} \pm 1$ are relevant. Since the

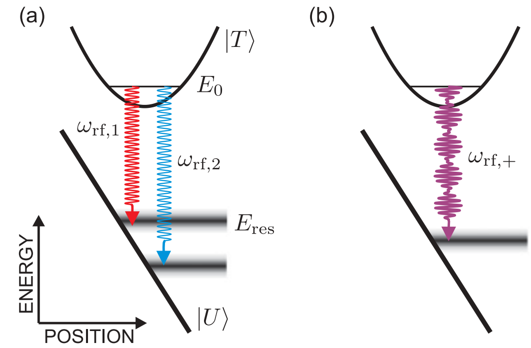

FIG. 1. (Color online) Schematic setup of potentials and couplings. The trapped Zeeman sublevel $|T\rangle$ is coupled to the untrapped level $|U\rangle$ by a weak rf field. Starting from a trapped state with energy E_0, the rf frequency determines the resonance energy E_{res}, around which a continuous spectrum of generalized energy eigenstates is populated during the output coupling. (a) With multiple simultaneous frequency components $\omega_{\text{rf},j}$, a corresponding set of resonant energy levels is formed. The atomic streams interfere as they fall in the gravity field. (b) Equivalently, the coupling can be interpreted as being driven by the sum of the single rf fields, which corresponds to a carrier frequency $\omega_{\text{rf},+} = (\omega_{\text{rf},1} + \omega_{\text{rf},2})/2$ and a coupling strength pulsing at frequency $\omega_{\text{rf},-} = (\omega_{\text{rf},1} - \omega_{\text{rf},2})/2$.

magnetic (trapping) potentials for the different sublevels are $\langle F,M_F|U_{\text{trap}}|F,M_F\rangle \propto \text{sgn}(g_F)M_F$, we assume that the trapped atoms are initially on the internal state $|T\rangle \equiv |F,M_F = \text{sgn}(g_F)\rangle$ and that the free-falling untrapped state is $|U\rangle \equiv |F,M_F = 0\rangle$. The transition between the internal states $|T\rangle \to |U\rangle$ is provided by the operator $F_{+/-}$ in systems with negative or positive g_F, respectively.

In the following, we neglect any population transfer to the antitrapped high-field-seeking Zeeman sublevels [$M_F = -n\,\text{sgn}(g_F)$, with $n = 1,\ldots,F$], for which the magnetic field minimum forms a repulsive potential, as well as to the more energetic trapped sublevels [$M_F = n\,\text{sgn}(g_F)$, with $n = 2,\ldots,F$]; the relevant potentials and couplings are illustrated in Fig. 1. This is a justified neglection since we are interested in the weak-coupling regime. On the other hand, if a maximal flux of atoms would be desirable, one would have to use strong rf fields, and in that case these neglected sublevels would have a nontrivial contribution [14]. With ever-stronger coupling strengths the system should be described by dressed potentials [35–38].

The convenient choice of basis functions depends on the internal state. For the trapped state $|T\rangle$, the basis is provided by the harmonic oscillator eigenstates $\{|\phi_n\rangle\}_{n=0}^\infty$. For the untrapped state $|U\rangle$, however, the external potential is linear, and the basis is formed by an uncountable set of generalized eigenfunctions, or distributions, $\{|\psi_E\rangle\}_{E\in\mathbb{R}}$, which satisfy the Airy differential equation [39]. Their explicit form is

$$\psi_E(x) = \mathcal{N}\text{Ai}[(x + E/mg)/l], \tag{5}$$

where the normalization factor $\mathcal{N} = 1/l\sqrt{mg}$ and the characteristic length scale $l = (\hbar^2/2gm^2)^{1/3}$. These generalized functions are not normalizable according to the L^2 norm, $\langle\psi_E|\psi_{E'}\rangle = \delta(E - E')$, and thus cannot individually represent any physical state. However, they form a complete orthonormal spatial basis in the sense that $\int dE\, \psi_E^*(x)\psi_E(x') = \delta(x - x')$. Therefore, any spatial state $|\varphi\rangle$ can be described in terms of these distributions as $|\varphi\rangle = \int dE\, f(E)|\psi_E\rangle$, where the spectrum is $f(E) = \langle\psi_E|\varphi\rangle$. Consequently, the normalization of the state is done in accordance with the properties of the spectrum, such that $\|\varphi\|^2 = \int dE\, |f(E)|^2$. It is immediately evident that any state $|\varphi_D,U\rangle$ described by a discrete spectrum $f(E) = \sum_i c_i\delta(E - E_i)$ is, first of all, unphysical and corresponds to a (quasi)periodic solution within the evolution generated by H_0. This does not fit with intuition about a free-fall event. Combining the previous statements, any state within our system can be expressed as

$$|\Psi(t)\rangle = \sum_n b_n(t)|\phi_n,T\rangle + \int dE\, c_E(t)|\psi_E,U\rangle. \tag{6}$$

In the interaction picture with respect to H_0, given by Eq. (2), $|\tilde{\Psi}(t)\rangle = e^{iH_0t/\hbar}|\Psi(t)\rangle$ and the corresponding coefficients are $\tilde{b}_n(t) = e^{iE_nt/\hbar}b_n(t)$ and $\tilde{c}_E(t) = e^{iEt/\hbar}c_E(t)$. In the following, we also use the notation $|\Psi_\beta\rangle \equiv \langle\beta|\Psi\rangle$, where $\beta = T,U$, for the trapped and untrapped components of the total state.

C. Wave-packet solution

The coupling between the different sublevels comes from interaction Hamiltonian (4). The weak coupling causes only a small perturbation in the bare system, defined by static Hamiltonian (2), and therefore its effect can be described by transition matrix elements. Let us assume that initially the system is at equilibrium in a trapped ground state $|\Psi(0)\rangle = |\phi,T\rangle$, for which $H_0|\phi\rangle = E_0|\phi\rangle$. In terms of representation (6), the coefficients are $b_0(0) = 1$, $b_n(0) = c_E(0) = 0$ for all $n > 0$ and $E \in \mathbb{R}$.

In the interaction picture, the equation of motion for the coefficients $\tilde{c}_E(t)$ is given by

$$\begin{aligned}\frac{d}{dt}\tilde{c}_E(t) &= \left\langle \psi_E,U \left| \frac{d}{dt}\tilde{\Psi}(t)\right.\right\rangle \\ &= -\frac{i}{\hbar}\langle\psi_E,U|\tilde{H}_I(t)|\tilde{\Psi}(t)\rangle \\ &= -\frac{i}{\hbar}\tilde{b}_0(t)e^{-i(E_0-E)t/\hbar}\langle\psi_E|\phi\rangle\langle U|H_I(t)|T\rangle. \end{aligned} \tag{7}$$

The trapped state remains essentially intact during the weak-coupling pulse, so we can assume $\tilde{b}_0(t) = 1$. The formal solution in the Schrödinger picture is

$$c_E(t) = -\frac{i}{\hbar}e^{-iEt/\hbar}\langle\psi_E|\phi\rangle\int_0^t ds\, e^{-i(E_0-E)s/\hbar}\langle U|H_I(s)|T\rangle. \tag{8}$$

Therefore, according to definition (6), the untrapped component is given by

$$\begin{aligned}|\Psi_U(t)\rangle = -\frac{i}{\hbar}\int_0^t ds\, e^{-iE_0s/\hbar}\langle U|H_I(s)|T\rangle \\ \times\int dE\, e^{-iE(t-s)/\hbar}\langle\psi_E|\phi\rangle|\psi_E\rangle.\end{aligned} \tag{9}$$

Defining the outcoupling rate function Ω and the respective instantaneous outcoupled state $|\Phi\rangle$, corresponding to a delta-peak outcoupling rate function, as

$$\Omega(t) \equiv -\frac{i}{\hbar}e^{-iE_0t/\hbar}\langle U|H_I(t)|T\rangle, \tag{10}$$

$$|\Phi(t)\rangle \equiv \int dE\, e^{-iEt/\hbar}\langle\psi_E|\phi\rangle|\psi_E\rangle = \langle U|e^{-iH_0t/\hbar}|\phi,U\rangle, \tag{11}$$

the full time-dependent solution for the outcoupled atomic beam can be written in a compact form as a convolution

$$|\Psi_U(t)\rangle = \int_0^t ds\, \Omega(s)|\Phi(t-s)\rangle = [\Omega * (\Theta|\Phi\rangle)](t), \tag{12}$$

where the Heaviside theta function, for which $\Theta(t)$ equals zero for $t < 0$ and unity for $t > 0$, takes care of a proper temporal causality. The instantaneous outcoupled state $|\Phi(t)\rangle$ matches the static-Hamiltonian-induced evolution [cf. Eq. (2)] of the spatial component of the initial trapped state $|\phi\rangle$, only its internal state is the untrapped one. Finally, we remind that $\Omega(t)$ vanishes for $t < 0$ according to our previous definition.

D. Continuous spectrum of states

Let us consider the matrix element of the interaction Hamiltonian between the trapped and untrapped states $\langle U|H_I|T\rangle$. Since the trapped and the untrapped states are separated by a single quantum of angular momentum, $\langle T|F_z|T\rangle = \mathrm{sgn}(g_F)\hbar = \pm\hbar$ and $\langle U|F_z|U\rangle = 0$, the transition between the states $|T\rangle \to |U\rangle$ is induced by the operator F_α, where $\alpha = +(-)$ for systems with negative (positive) g_F. Therefore, Eq. (7) is

$$\begin{aligned}\frac{d}{dt}\tilde{c}_E(t) = -\frac{i}{2\sqrt{2}\hbar^2}\mu_0 g_F B_0(t)\langle\psi_E|\phi\rangle\langle U|F_\alpha|T\rangle \\ \times\{(\hat{\mathbf{e}}_\alpha^*\cdot\hat{\mathbf{e}}_{\mathrm{rf}})e^{-i[(E_0+\omega_{\mathrm{rf}}-E)t+\theta]} \\ +(\hat{\mathbf{e}}_\alpha^*\cdot\hat{\mathbf{e}}_{\mathrm{rf}}^*)e^{-i[(E_0-\omega_{\mathrm{rf}}-E)t-\theta]}\},\end{aligned} \tag{13}$$

where the factor $\sqrt{2}$ comes from the identity $\hat{\mathbf{e}}_\pm\cdot\mathbf{F} = F_\pm/\sqrt{2}$.

With a constant rf field, $B_0(t) = B_0\Theta(t)$, the time integration gives the terms

$$\tilde{c}_E(t) \propto t\langle\psi_E|\phi\rangle\mathrm{sinc}\left(\frac{E_0\pm\omega_{\mathrm{rf}}-E}{2}t\right). \tag{14}$$

Therefore, the spectrum concentrates in the vicinity of resonant energy levels $E = E_0 \pm \omega_{\mathrm{rf}}$ as time passes. According to the physical setup, on the other hand, the overlap integral $\langle\psi_E|\phi\rangle$ is concentrated around $E \simeq -mg\langle\phi|x|\phi\rangle \ll E_0$. Consequently, the significant contribution accumulates around the resonant energy level

$$E_{\mathrm{res}} \equiv E_0 - \omega_{\mathrm{rf}}. \tag{15}$$

In terms of the generalized eigenstates, there will always be a continuous range of occupied states around the resonant energy E_{res}.

III. VISIBILITY OF THE INTERFERENCE PATTERN

The form of the free-falling atomic cloud $|\Psi_U\rangle$ was expressed in Eq. (12) as a convolution of the outcoupling rate function $\Omega(t)$ and a spatial term $|\Phi(t)\rangle$. Next we consider the emerging interference patterns due to multiple rf fields driving the coupling simultaneously.

The corresponding (classical) magnetic field components $\mathbf{B}^i_{\rm rf}(t)$ interfere with each other, such that the total field is $\mathbf{B}_{\rm rf}(t) = \sum_i \mathbf{B}^i_{\rm rf}(t)$. Correspondingly, the outcoupling rate function $\Omega(t) = \sum_i \Omega_i(t)$ and, because of the linearity of Eq. (12), the outcoupled component is

$$|\Psi_U(t)\rangle = [\Omega * (\Theta|\Phi\rangle)](t) = \sum_i [\Omega_i * (\Theta|\Phi\rangle)](t) = \sum_i |\Psi^i_U(t)\rangle. \quad (16)$$

The interference pattern appears similarly in the (quantum) matter fields as a sum of atomic streams, each of which corresponds to an atomic beam outcoupled by a single rf-field component.

A. Interference of classical fields

The point of view expressed in Ref. [33] was that the combination of the (classical) magnetic fields, which operate at frequencies ω_1 and ω_2 with equal constant amplitudes, corresponds to a single field whose carrier frequency is the average $\omega_+ = (\omega_1 + \omega_2)/2$ and the pulse envelope is modulated at frequency $\omega_- = (\omega_1 - \omega_2)/2$ (cf. Fig. 1). Moreover, the relative phase difference between the circular components driving the outcoupling,

$$\Delta\theta = \arg(\hat{\mathbf{e}}^*_\alpha \cdot \hat{\mathbf{e}}^*_{\rm rf,1} e^{i\theta_1}) - \arg(\hat{\mathbf{e}}^*_\alpha \cdot \hat{\mathbf{e}}^*_{\rm rf,2} e^{i\theta_2}), \quad (17)$$

shifts the envelope of the interference pattern and, consequently, the intensity profile of the falling stream of atoms. Generally, the interference pattern depends on (i) the relative amplitudes, (ii) the relative phase difference, and (iii) frequency separation.

Based on this description, one might expect that whenever the carrier frequency ω_+ falls into the region where the overlap integral $|\langle\psi_{E_0-\hbar\omega_+}|\phi\rangle|$ is finite, there would be a finite stream of atoms falling from the trap, and the intensity of the stream would be modulated at frequency ω_-, such that the maxima of the rf field coincide with the maxima of the atomic intensity (see Fig. 3 in Ref. [33]).

B. Interference of quantum fields

The wave-packet result derived in Sec. II C explains why the above-mentioned simplistic analogy from the classical interference is not exactly true. According to Eq. (16), the visibility of the interference pattern is affected by two contributions: (i) the interference pattern of the magnetic fields and (ii) the convolution by the temporal free-fall evolution of the initial trapped-state profile. If we look at the stream at a particular position x as a function of time, the interference pattern of the magnetic fields, possibly with perfect visibility, is smoothed by the temporal width of the instantaneous outcoupled state $|\Phi(x,t)\rangle$ falling past this point.

For a Gaussian initial state $|\phi_0\rangle$, the analytical solution

$$|\Phi(x,t)\rangle \propto \exp\left[-\frac{\left(x - x_0 - \frac{1}{2}gt^2\right)^2}{2\sigma(t)^2}\right], \quad (18)$$

where $x_0 = g/\omega^2$ and $\sigma(t) = \sqrt{\sigma_0^2 + t^2/\sigma_0^2}$, with $\sigma_0 = \sqrt{\hbar/m\omega}$, allows us to estimate the temporal width. Namely, at time t the wave packet has a spatial width of $\sigma(t)$ centralized around position $x_0 + \frac{1}{2}gt^2$, and the center of mass falls with velocity $v(t) = gt$, so the passing time is approximately $\sigma(t)/v(t) \geqslant 1/\sigma g$; this value corresponds to a balance between dispersion and gravitational acceleration. Therefore, even with an infinitely long coupling time, the interference pattern is still smoothed by a distribution with a finite width.

With a single rf field, the amplitude of the falling atomic flux depends on the applied rf frequency $\omega_{\rm rf}$. This can be seen from resonance energy condition (15) as compared to the overlap integral $\langle\psi_E|\phi\rangle$. Therefore, two different rf frequencies generally produce atomic streams with different amplitudes, even if the rf-field amplitudes are the same. According to Eq. (16), the relative phase difference of two magnetic fields [Eq. (17)] maps directly to the relative phase difference of the resulting matter waves. This was explicitly demonstrated in the experiment of Ref. [33].

TABLE I. Physical parameters used in the examples. Here $a_0 = 5.5 \times 10^{-11}$ m is the Bohr radius.

Quantity	Symbol	Value
Trap frequency (x and z directions)	$\omega_{x,z}/2\pi$	160 Hz
Trap frequency (y direction)	$\omega_y/2\pi$	6.7 Hz
Rabi frequency	$\lvert\Omega\rvert/2\pi$	50 Hz
Bias frequency	$\omega_{\rm bias}/2\pi$	900 kHz
Number of atoms	N	10^5
Scattering length	a	103 a_0

IV. APPLICATION AND COMPARISON TO NUMERICAL RESULTS

In the following, we concentrate on ^{87}Rb atoms and in particular the hyperfine ground state $F = 1$. In this case the Landé factor is $g_F = -1/2$ and, therefore, the trapped low-field-seeking Zeeman sublevel is $|T\rangle = |F = 1, M_F = -1\rangle$ and the untrapped one is $|U\rangle = |F = 1, M_F = 0\rangle$ (see Fig. 1). The physical parameters are adopted from Ref. [33] and are summarized in Table I.

In this section we compare wave-packet solution (12) to numerical simulations including all the Zeeman sublevels. Especially we show the impact of the atomic contact interactions

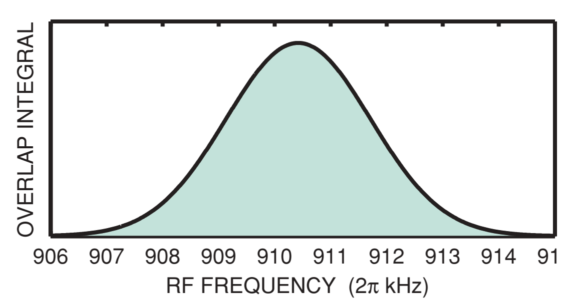

FIG. 2. (Color online) The overlap integral $\langle\psi_{E_0-\hbar\omega_{\rm rf}}|\phi_0\rangle$, in arbitrary units, as a function of rf frequency $\omega_{\rm rf}$. As mentioned in the text, the form is well approximated by a Gaussian shape centralized at $(E - mgx_0)/h \simeq 910.3$ kHz with width $mg\sigma/h \simeq 1.8$ kHz.

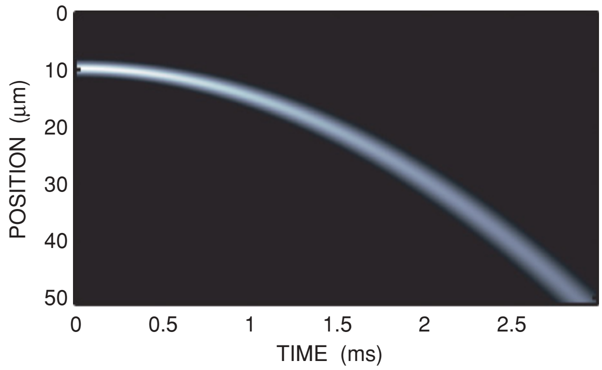

FIG. 3. (Color online) The density profile of the instantaneous outcoupled state $|\Phi(x,t)|^2$ (arbitrary units). Initially the state is the Gaussian ground state of a harmonic potential. In the linear potential slope the functional form is maintained, while the center of mass accelerates according to classical mechanics, $x_0(t) = x_0 + \frac{1}{2}gt^2$, and the width disperses, $\sigma^2(t) = \sigma_0^2 + t^2/\sigma_0^2$.

by solving the corresponding Gross-Pitaevskii equation [4,5]. Both the model and the simulations are one dimensional (1D). The contact interactions appear as an additional nonlinear mean-field term $U_{\rm int}(x,t) = g_{\rm 1D}|\Psi(x,t)|^2$. The scaled interaction coefficient is $g_{\rm 1D} = (\sqrt{\omega_1\omega_2}m/2\pi\hbar)g_{3D}$ [40], where the three-dimensional (3D) interaction term is $g_{\rm 3D} = 4\pi\hbar^2 aN/m$, with scattering length a and number of particles N [4,5].

When neglecting the atomic contact interactions, the ground state of the harmonic trapping potential is a Gaussian $|\phi_0\rangle$. The overlap integral between the Gaussian state and the generalized energy eigenstates $|\psi_E\rangle$ can be calculated analytically [19,23]. In the limit of a steep gravity slope, $g \gg 0$, the generalized energy eigenfunction approaches Dirac's δ distribution as $|\psi_E(x)\rangle \sim \delta(x + E/mg)/\sqrt{mg}$. Since the width of the trapped state σ clearly exceeds the characteristic length scale of the Airy distribution l, the overlap integral is well approximated by $\langle\psi_E|\phi_0\rangle \simeq [\pi(mg\sigma)^2]^{-1/4}\exp[-(E+mgx_0)^2/2(mg\sigma)^2]$, as is obvious in Fig. 2.

In Fig. 3 the time evolution of the instantaneous outcoupled state (11) for the noninteracting case is shown. The state

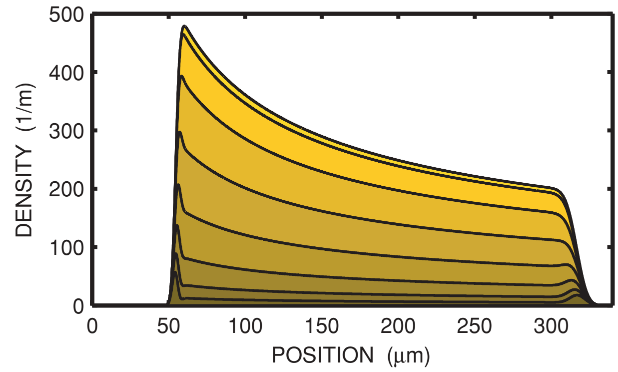

FIG. 5. (Color online) Output-coupled atomic density profiles 8 ms after the beginning of a 5-ms-long box-shaped pulse. The plot shows eight different rf frequencies, from lowest to highest density: $\omega_{\rm rf}/2\pi = 907, 907.5, \ldots, 910.5$ kHz (cf. Fig. 2).

corresponds to falling atoms outcoupled by an infinitesimally short rf pulse. The total wave packet due to an rf pulse with a finite duration is achieved by integrating this state over time, in accordance with Eq. (12). In the examples, we use a 5-ms-long box-shaped pulse form for the rf field. The field amplitude is such that the maximum Rabi frequency is $|\Omega|/2\pi = 50$ Hz. However, in the spirit of Ref. [33], we assume linear polarization and the coupling is therefore suppressed by a factor of $1/\sqrt{2}$. The density profile of the resulting stream of outcoupled atoms versus time is shown in Fig. 4. The number of outcoupled atoms, as well as the density profile, depends on the applied rf frequency. This dependency is shown in Fig. 5. The increase in the density follows the amplitude of the overlap integral shown in Fig. 2.

The density profile of a pulsating outcoupled stream, which is produced by two simultaneous resonant rf pulses separated in frequency by $\Delta\omega_{\rm rf}/2\pi = 1$ kHz and in phase by $\Delta\theta = \pi$, is shown in Fig. 6 as a function of time. In Fig. 7 we compare the analytically calculated density profile to the numerically computed one. In the numerical computation the time-dependent Schrödinger equation was evolved, taking into account three states: one harmonically trapped, one harmonically antitrapped, and one

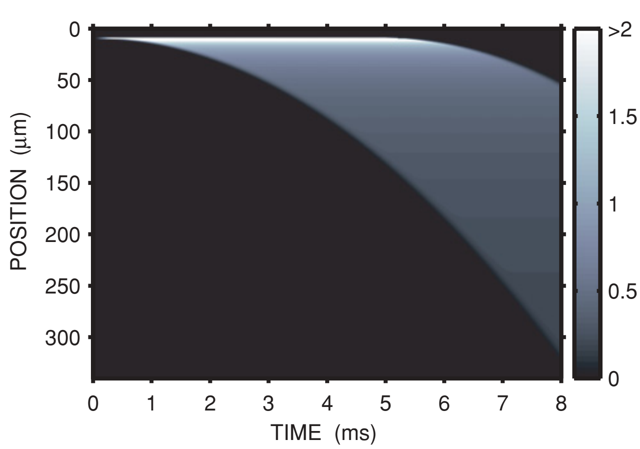

FIG. 4. (Color online) Output-coupled atomic density for a 5-ms-long box-shaped pulse with rf frequency $\omega_{\rm rf}/2\pi = 910$ kHz. The density is in units of 10^3 m^{-1} and is flattened from above to increase clarity.

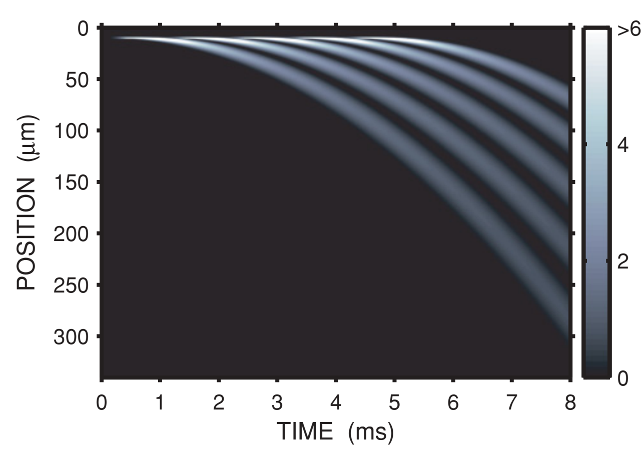

FIG. 6. (Color online) As Fig. 4 but with two simultaneous equally strong pulses with rf frequencies $\omega_{\rm rf,1}/2\pi = 910$ kHz and $\omega_{\rm rf,1}/2\pi = 911$ kHz, and with a relative phase difference of π.

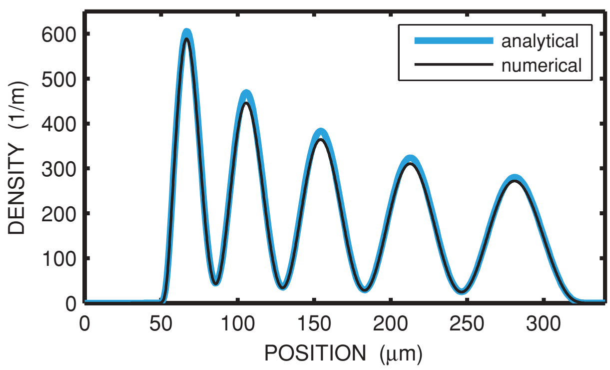

FIG. 7. (Color online) As Fig. 5, but with two simultaneous rf fields with $\omega_{\mathrm{rf},1}/2\pi = 909$ kHz and $\omega_{\mathrm{rf},2}/2\pi = 908$ kHz, and a relative phase difference of π. Analytical model (thick line) agrees well with numerical simulation (thin line).

affected by a linear potential with the slope corresponding to the gravity. The numerical computations were done for both interacting and noninteracting cases. Overall, we find good agreement between the analytical and the numerical results.

Due to the atomic contact interactions, the trapped ground state is broadened from a Gaussian into a Thomas-Fermi distribution. Accordingly, the range of radio frequencies capable of producing outcoupling changes. In Fig. 8 we show how, also in the interacting case, the visibility of the interference pattern due to two equally strong rf fields is not perfect. In particular, our example shows the interesting case where one of the rf frequencies outcouples hardly any stream while the other one and the average do. As in the noninteracting case, applying the equally strong fields simultaneously produces interference with low visibility.

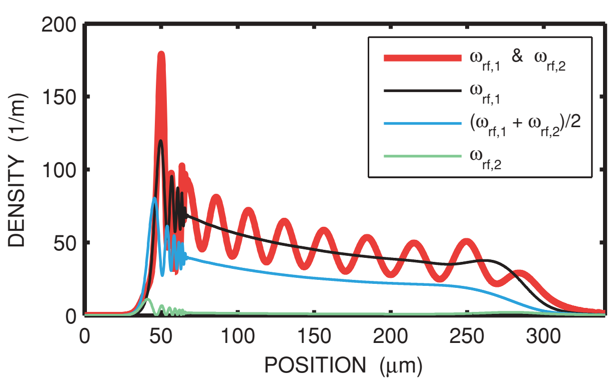

FIG. 8. (Color online) As Fig. 5, but including the atomic contact interactions. Looking at the outcoupling near the edge of the distribution, there is a situation, where one rf frequency ($\omega_{\mathrm{rf},1}/2\pi =$ 903 kHz, highest thin straight line) produces a strong stream of atoms, another rf frequency ($\omega_{\mathrm{rf},2}/2\pi = 901$ kHz, lowest thin straight line) with the same field amplitude almost nothing, and the average rf frequency $(\omega_{\mathrm{rf},1} + \omega_{\mathrm{rf},2})/2$ (middle thin straight line) again a clear stream. Applying both equally strong fields simultaneously, with a relative phase difference of π, shows interference with a limited visibility (thick oscillating line) in accordance with the noninteracting examples.

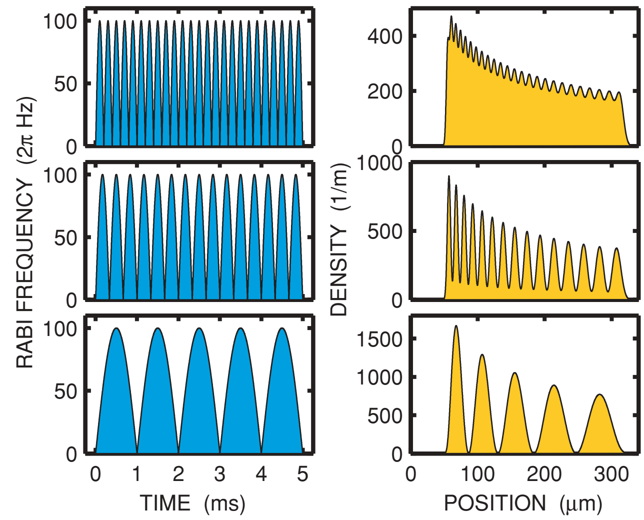

FIG. 9. (Color online) The perfect interference patterns of the coupling magnetic fields (left panels) map to smoothed interference in the corresponding atomic density (right panels) because of the finite spatial extent of the trapped state. The frequencies used are $\omega_{\mathrm{rf},1}/2\pi = 911$ kHz and (i) $\omega_{\mathrm{rf},2}/2\pi = 906$ kHz (top row) (ii) $\omega_{\mathrm{rf},2}/2\pi = 908$ kHz (middle row), and (iii) $\omega_{\mathrm{rf},2}/2\pi = 910$ kHz (bottom row). The relative phase difference between the 5-ms-long pulses is π and the atomic density is plotted at time $t = 8$ ms.

Finally, in Fig. 9, we compare the rf pulses and induced outcoupling streams. The figure clearly shows how the visibility in the outcoupled atomic stream diminishes with increasing frequency separation in the causative outcoupling rf fields, even if the rf field itself is with perfect visibility.

V. CONCLUSIONS AND DISCUSSION

We have derived a linear wave-packet solution for an output coupling scenario. The model establishes a bridge between two different ways of looking at the interference of overlapping atom lasers and shows that the effect can be understood equally as interference of spatially extended atomic clouds as well as interference of classical magnetic fields causing the output coupling.

The model is built in terms of generalized energy eigenstates of a linear potential caused by gravity, and it shows how the total wave packet can be interpreted as being constructed by a continuous loading of a continuous spectrum of these states, which individually do not correspond to a physical solution. In general, our model does not suffer from unphysical infinite quantities [21,31].

Through the analysis of the solution, it was shown that the visibility of the observed interference pattern is limited by the spatial extent of the trapped cloud, which serves as a source for the atomic beams. Furthermore, the visibility is shown to be affected by the rf frequencies in the sense of selecting a resonant energy and, moreover, amplitude for the atomic stream.

The simple linear model was then compared to numerical simulations including the atomic interactions as well as all the Zeeman sublevels, and the qualitative match was shown to be excellent using experimentally realistic parameters. The model is one dimensional and assumes weak coupling. The applicability is therefore restricted to cases where the transversal extent of the source condensate is wide [11,23,24]. Within these restrictions, the presented linear model also generalizes straightforwardly for multiple dimensions and to an outcoupling scenario based on a Raman transition including an initial momentum kick.

ACKNOWLEDGMENTS

Financial support from the National Graduate School of Modern Optics and Photonics (K.H.), the Turku University Foundation (K.H.), the Finnish Cultural Foundation (O.V.), and the Academy of Finland (Project Nos. 115682 and 122595) is gratefully acknowledged. Also, we wish to thank the Extensible Multi-Dimensional Simulator team (www.xmds.org) for providing means for fast and easy numerical computing.

[1] M. H. Anderson, J. R. Ensher, M. R. Matthews, C. E. Wieman, and E. A. Cornell, Science **269**, 198 (1995).

[2] K. B. Davis, M.-O. Mewes, M. R. Andrews, N. J. van Druten, D. S. Durfee, D. M. Kurn, and W. Ketterle, Phys. Rev. Lett. **75**, 3969 (1995).

[3] C. C. Bradley, C. A. Sackett, J. J. Tollett, and R. G. Hulet, Phys. Rev. Lett. **75**, 1687 (1995).

[4] C. J. Pethick and H. Smith, *Bose-Einstein Condensation in Dilute Gases* (Cambridge University Press, Cambridge, England, 2002).

[5] L. Pitaevskii and S. Stringari, *Bose-Einstein Condensation* (Oxford University Press, Oxford, 2003).

[6] M.-O. Mewes, M. R. Andrews, D. M. Kurn, D. S. Durfee, C. G. Townsend, and W. Ketterle, Phys. Rev. Lett. **78**, 582 (1997).

[7] M. R. Andrews, C. G. Townsend, H.-J. Miesner, D. S. Durfee, D. M. Kurn, and W. Ketterle, Science **275**, 637 (1997).

[8] A. Öttl, S. Ritter, M. Köhl, and T. Esslinger, Phys. Rev. Lett. **95**, 090404 (2005).

[9] I. Bloch, T. W. Hänsch, and T. Esslinger, Phys. Rev. Lett. **82**, 3008 (1999).

[10] M. Köhl, T. W. Hänsch, and T. Esslinger, Phys. Rev. Lett. **87**, 160404 (2001).

[11] Y. B. Band, P. S. Julienne, and M. Trippenbach, Phys. Rev. A **59**, 3823 (1999).

[12] F. Gerbier, P. Bouyer, and A. Aspect, Phys. Rev. Lett. **86**, 4729 (2001).

[13] N. V. Vitanov and K.-A. Suominen, Phys. Rev. A **56**, R4377 (1997).

[14] N. P. Robins, A. K. Morrison, J. J. Hope, and J. D. Close, Phys. Rev. A **72**, 031606(R) (2005).

[15] E. W. Hagley, L. Deng, M. Kozuma, J. Wen, K. Helmerson, S. L. Rolston, and W. D. Phillips, Science **283**, 1706 (1999).

[16] B. P. Anderson and M. A. Kasevich, Science **282**, 1686 (1998).

[17] K.-A. Suominen, B. M. Garraway, and S. Stenholm, Phys. Rev. A **45**, 3060 (1992).

[18] B. M. Garraway and K.-A. Suominen, Rep. Prog. Phys. **58**, 365 (1995).

[19] A. Paloviita, K.-A. Suominen, and S. Stenholm, J. Phys. B **30**, 2623 (1997).

[20] J. Schneider and A. Schenzle, Appl. Phys. B **69**, 353 (1999).

[21] J. Schneider and A. Schenzle, Phys. Rev. A **61**, 053611 (2000).

[22] J. Dugué, N. P. Robins, C. Figl, M. Jeppesen, P. Summers, M. T. Johnsson, J. J. Hope, and J. D. Close, Phys. Rev. A **75**, 053602 (2007).

[23] T. Kramer and M. Rodríguez, Phys. Rev. A **74**, 013611 (2006).

[24] T. Kramer, C. Bracher, and K. Kleber, J. Phys. A **35**, 8361 (2002).

[25] Y. Japha, S. Choi, K. Burnett, and Y. B. Band, Phys. Rev. Lett. **82**, 1079 (1999).

[26] S. Choi, Y. Japha, and K. Burnett, Phys. Rev. A **61**, 063606 (2000).

[27] S. A. Haine, J. J. Hope, N. P. Robins, and C. M. Savage, Phys. Rev. Lett. **88**, 170403 (2002).

[28] S. A. Haine and J. J. Hope, Phys. Rev. A **68**, 023607 (2003).

[29] N. Robins, C. Savage, and E. A. Ostrovskaya, Phys. Rev. A **64**, 043605 (2001).

[30] A. del Campo, J. G. Muga, and M. Moshinsky, J. Phys. B **40**, 975 (2007).

[31] I. Bloch, T. W. Hänsch, and T. Esslinger, Nature (London) **403**, 166 (2000).

[32] T. Bourdel, T. Donner, S. Ritter, A. Öttl, M. Köhl, and T. Esslinger, Phys. Rev. A **73**, 043602 (2006).

[33] O. Vainio, C. J. Vale, M. J. Davis, N. R. Heckenberg, and H. Rubinsztein-Dunlop, Phys. Rev. A **73**, 063613 (2006).

[34] B. H. Bransden and C. J. Joachain, *Physics of Atoms and Molecules*, 2nd ed. (Pearson Education, Harlow, 2003).

[35] O. Zobay and B. M. Garraway, Phys. Rev. Lett. **86**, 1195 (2001).

[36] O. Zobay and B. M. Garraway, Phys. Rev. A **69**, 023605 (2004).

[37] T. Schumm, S. Hoffenberth, L. M. Andersson, S. Wildermuth, S. Groth, I. Bar-Joseph, J. Schmiedmayer, and P. Krüger, Nature Phys. **1**, 57 (2005).

[38] S. Hofferberth, I. Lesanovsky, B. Fischer, J. Verdu, and J. Schmiedmayer, Nature Phys. **2**, 710 (2006).

[39] M. Abramowitz and I. A. Stegun, *Handbook of Mathematical Functions* (Dover, New York, 1970).

[40] D. S. Petrov, D. M. Gangardt, and G. V. Shlyapnikov, J. Phys. IV (France) **116**, 5 (2004).